Lithium−Nickel Citrate Precursors for the Preparation of $LiNiO_2$ Insertion Electrodes

R. Alcántara, P. Lavela, and J. L. Tirado*

Laboratorio de Química Inorgánica, Facultad de Ciencias, Universidad de Córdoba, Avda. San Alberto Magno s/n. 14004 Córdoba, Spain

R. Stoyanova, E. Kuzmanova, and E. Zhecheva

Institute of General and Inorganic Chemistry, Bulgarian Academy of Sciences, 1113 Sofia, Bulgaria

Received April 17, 1997. Revised Manuscript Received July 21, 1997[⊗]

Noncrystalline solids with $LiNi(C_6H_4O_7)_{3/4}\cdot xH_2O$, $LiNi(C_6H_5O_7)\cdot xH_2O$, and $(NH_4)_3LiNi(C_6H_5O_7)_2\cdot xH_2O$ ($x \approx 5$) chemical compositions were obtained by freeze drying of concentrated lithium−nickel−citrate solutions. The IR spectra of solid citrates reveal that triionized citrate ions chelate the Ni^{2+} ions with their carboxylate groups acting as monodentate agents. Electronic spectra reveal monomeric 1:1 Ni(II)−citrate(−3) complexes in the mixed citrate powders. Finely disperse layered $Li_{1-x}Ni_{1+x}O_2$ solids were obtained by the thermal decomposition of the citrate precursors at 700−800 °C in an oxygen atmosphere. Almost stoichiometric $Li_{1-x}Ni_{1+x}O_2$ ($x \leq 0.05$) oxides with layered $R\bar{3}m$ structure are obtained from monocitrate precursors. The $LiNiO_2$ powder were used as active cathode material in lithium cells. Cyclic voltammograms showed several current peaks during the first cycle resulting from the formation of the intermediate phases usually found in quasi-stoichiometric $LiNiO_2$. After the almost complete extraction of lithium, further cycles reveal a significant loss of capacity and changes in the number of current peaks as a result of the changes induced in the structure of the solid. EPR data on cycled $LiNiO_2$ show partial migration of Ni from 3a (nickel layers) to 3b sites (lithium layers).

1. Introduction

Lithium cobalt and nickel oxides, $LiMO_2$, as well as lithium manganese spinel oxides, $Li_{1+x}Mn_2O_4$, have been shown to belong to the most promising 4 V cathode materials for lithium-ion cells. Although some commercial batteries for portable applications already use these materials,[1] research is actively devoted to improve the preparation procedures and electrochemical properties of the oxides. The soft-chemistry methods for materials design enable the preparation of ultrafine materials with controlled composition, structure, and morphology. In this way, soft-chemistry methods provide the possibilities for the elaboration of high-rate electrodes that show good cycling behavior at high charge/discharge rates.[2−4] The main concept of the various soft-chemistry methods is a chemical design of precursors where the different constituents are fixed at microscale level.

Summarizing the literature data on the low-temperature preparation of $LiMn_2O_4$ and $LiCoO_2$, three variants of the soft-chemistry methods have to be pointed out: sol−gel processes, metal−organic precursors, and ion-exchange reactions. For example, the Peccini's variety of the citrate method was recently adopted in the synthesis of the spinel $LiMn_2O_4$: ethylene glycol is used to polyesterify the citrate complexes of Mn and Li into cross-linked polymer resin, which decomposes above 250 °C.[5] Moreover, $LiMn_2O_4$ spinel has been obtained via the reduction of an aqueous lithium permanganate solution by fumaric acid.[6] Oh et al.[7] have recently communicated a sol−gel method using polyacrylic acid as a chelating agent in the preparation of ultrafine high-temperature $LiCoO_2$. Lithium−manganese−organic precursors such as acetates,[8] oxalates,[9] succinates,[9] malonates,[9] tartrates,[10] citrates,[11,12] and glycolates[13,14] decompose at temperatures above 300 °C leading to the formation of $LiMn_2O_4$ spinels. For $LiCoO_2$, hydroxide−acetate,[8] hydroxide,[15,16] glycolate,[13,14] and succinate and malate[17] synthesis routes have been developed. The

[⊗] Abstract published in *Advance ACS Abstracts*, September 1, 1997.

(1) Nagaura, T. *Prog. Batteries Battery Mater.* **1991**, *10*, 209.
(2) Dunn, B.; Farrington, G. C.; Katz, B. *Solid State Ionics* **1994**, *70/71*, 3.
(3) Sleich, D. M. *Solid State Ionics* **1994**, *70/71*, 407.
(4) Pereira-Ramos, J. P. *J. Power Sources* **1995**, *54*, 120.
(5) Li, W.; Farrington, G. C.; Chaput, F.; Dunn, B. *J. Electrochem. Soc.* **1996**, *143*, 879.
(6) Bach, S.; Henry, M.; Baffier, N.; Livage, J. *J. Solid State Chem.* **1990**, *88*, 325.
(7) Sun, Y.-K.; Oh, I.-H.; Hong, S. A. *J. Mater. Sci.* **1996**, *31*, 3617.
(8) Barboux, P.; Tarascon, J. M.; Shokoohi, F. K. *J. Solid State Chem.* **1991**, *94*, 185.
(9) Tsumura, T.; Kishi, S.; Konno, H.; Shimizu, A.; Inagaki, M. *Thermochim. Acta* **1996**, *278*, 135.
(10) Tsumura, T.; Shimizu, A.; Inagaki, M. *J. Mater. Chem.* **1993**, *3*, 995.
(11) Prabaharan, S. R. S.; Michael, M. S.; Kumar, T. P.; Mani, A.; Athinarayanaswamy, K.; Gangadharan, R. *J. Mater. Chem.* **1995**, *5*, 1035.
(12) Yasushi, H., Nippondenso Co., Ltd., U.S. Patent 5,565,688, 1996.
(13) Fragnaud, P.; Schleich, D. M. *Sensors Actuators* **1995**, *A51*, 21.
(14) Fragnaud, P.; Nagarajan, R.; Schleich, D. M.; Vujic, D. *J. Power Sources* **1995**, *54*, 362.
(15) Garcia, B.; Barboux, P.; Ribot, F.; Kahn-Harari, A.; Mazerolles, L.; Baffier, N. *Solid State Ionics* **1995**, *80*, 111.
(16) Garcia, B.; Farcy, J.; Pereira-Ramos, J.-P.; Perichon, J.; Baffier, N. *J. Power Sources* **1995**, *54*, 373.

S0897-4756(97)00236-6 CCC: $14.00

ion-exchange reaction between H^+ from γ-MnOOH with Li^+ from concentrated LiOH aqueous solution is a new synthesis route for the preparation of orthorhombic $LiMnO_2$.[18]

In contrast to $LiMn_2O_4$ and $LiCoO_2$, the use of low-temperature techniques for the synthesis of $LiNiO_2$ is limited due to the difficulties in the stabilization of Ni^{3+}.[19] Nevertheless, there is a communication on the formation of monodisperse $LiNiO_2$ (at 750 °C for short heating time) by applying the sol−gel process where poly(vinyl butyral) serves as a chelating agent.[20] Barboux et al.[8] have tried to prepare $LiNiO_2$ by solutions techniques using hydroxide−acetates as precursors, but their reaction product was always NiO and Li_2CO_3. Furthermore, acetate and hydroxide−succinate methods in the preparation of lithium nickelates have also been reported.[21] To the best of our knowledge, organic polyfunctional acids are not used for the preparation of stoichiometric $LiNiO_2$.

Lithium nickelate, $LiNiO_2$, possesses the trigonal crystal structure where Li^+ and Ni^{3+} ions occupy alternatively the octahedral sites in the close packing of oxygen atoms, thus building LiO_2 and NiO_2 layers (space group $R3m$). In contrast to $LiCoO_2$, the Li−Ni−O system forms solid solutions, $Li_{1-x}Ni_{1+x}O_2$, for the whole range of $0 < x < 1$ whereby at $x \sim 0.35$ a disorder−order transition from the rock-salt to the layered trigonal structure appears.[19,22] Systematic investigations on the electrochemical properties of $Li_{1-x}Ni_{1+x}O_2$ compositions have shown that lithium nickelate with a lithium content close to 1 displays a high capacity and a good reversibility toward the lithium intercalation/deintercalation reactions.[23−26] Owing to the high volatility of the lithium salts, the preparation of $Li_{1-x}Ni_{1+x}O_2$ compositions with $x \rightarrow 0$ is a complicated procedure. In addition, during prolonged heating at high temperatures (above 700 °C), stoichiometric $LiNiO_2$ decomposes to $Li_{1-x}Ni_{1+x}O_2$ with $x > 0$.[27] To prepare stoichiometric lithium nickelate, lithium in excess of the stoichiometric amount is usually taken. The excess of lithium that does not sublimate during the solid-state reaction is washed away with water or alcohol. Thus, nearly stoichiometric $Li_{0.995}Ni_{1.005}O_2$ has been prepared at 700 °C in air from $LiOH{\cdot}H_2O$ and $Ni(NO_3)_2{\cdot}6H_2O$ using a 4-fold excess of lithium (Li:Ni = 4:1).[24] Using a 10% excess of lithium, Reimers et al. have prepared from NiO and $LiOH{\cdot}H_2O$ nearly stoichiometric $LiNiO_2$ at 650 °C and have characterized their product by neutron diffraction.[28] The highly reactive Li_2O and Li_2O_2, taken in stoichiometric amounts, yield at 700 °C in an oxygen atmosphere or in an oxygen gas flow $Li_{1-x}Ni_{1+x}O_2$ compositions with a lithium content $(1 - x) = 0.98-0.99$.[25,26]

Recently, we have elaborated a new citrate method for the preparation, even at 400 °C, of $LiCoO_2$ characterized with a trigonal crystal structure and consisting of hexagonal particles with a diameter of 70−120 nm.[29,30] This method consists of thermal pyrolysis of homogeneous lithium−cobalt−citrate compositions obtained by ethanol dehydration or freeze-drying of the corresponding aqueous solutions. Atomic scale mixing of Li and Co is achieved with citric acid acting as a chelating agent. Taking into account the citrate method for $LiCoO_2$ synthesis, citric acid, $HOOCCH_2C(OH)(COOH)CH_2COOH \equiv Cit$, seems to be a suitable chelating agent also for the preparation of $LiNiO_2$. In aqueous solutions at $6 < pH < 8$, as in the case of most other bivalent transition-metal ions, Ni^{2+} form mainly 1:1 and 1:2 citrate(−3) complexes: $[NiCit]^-$ and $[NiCit_2]^{4-}$.[31] Above pH = 8, nickel−citrate complexes with the tetraionized acid, $[NiCit]^{2-}$, appear, whereas Ni−hydroxide−citrate(−4) complexes, $[Ni(OH)_nCit]^{-(2+n)}$ ($n = 1, 2, 3$), are also formed at pH > 9.[32,33] The complex formation between Co and citric acid via polyfunctional groups allows us to obtain and to modify the metal−organic precursors at a molecular level.

With this study we have adapted the citrate method for the preparation of $LiNiO_2$. One of the important features of this method is that the lithium and nickel are in stoichiometric amount in the Li−Ni−citric acid solutions. Moreover, by variation in the Ni/Cit ratio in the precursors, we were able to control the composition of $LiNiO_2$. In an attempt to monitor the cation distribution in $LiNiO_2$ derived from citrate precursors, EPR measurements of low-spin Ni^{3+} were undertaken.

2. Experimental Section

2.1. Preparation of Lithium−Nickel Citrate Precursors. For the preparation of lithium−nickel−citrate solutions, $Ni(OH)_2$ was dissolved in 0.1 M citric acid at 80 °C. When a transparent solution was observed, a saturated $LiOH{\cdot}H_2O$ solution was added, the molar ratio between the components being as follows: Li:Ni:Cit = l:1:0.75 (solution a), Li:Ni:Cit = l:1:1 (solution b), and Li:Ni:Cit = l:1:2 (solution c). The pH value of solution (a) thus obtained was 8.5, whereas for solutions (b) and (c) ammonia was added up to pH = 6.5. The lithium−nickel−citrate solutions were concentrated to 0.5 M Ni. After complexation, the solutions were cooled to room temperature, then frozen instantly with liquid nitrogen and dried in vacuum (20−30 mbar) at −20 °C with an Alpha-Crist freeze-dryer. For the sake of simplicity, the freeze-dried compositions will be denoted as $LiNiCit_{3/4}$, LiNiCit, and $LiNiCit_2$. For some experiments, a solution (b) with a nickel concentration of 0.05 M was also subjected to freeze-drying (sample denoted as $LiNiCit_{0.05M}$). After drying, the solid residues were heated to 500 °C in air with a heating rate of 1 °C/min and then annealed at 700 or 800 °C for 20 and 40 h in

(17) Yoshio, M.; Tanaka, H.; Tominaga, K.; Noguchi, H. *J. Power Sources* **1992**, *40*, 347.
(18) Reimers, J. N.; Fuller, E. W.; Rossen, E.; Dahn, J. R. *J. Electrochem. Soc.* **1993**, *140*, 3396.
(19) Goodenough, J. B.; Wickham, D. G.; Croft, W. J. *J. Phys. Chem. Solids* **1958**, *5*, 107.
(20) Sun, Y.-K.; Oh, I.-H. *J. Mater. Sci.* **1997**, *16*, 30.
(21) Noguchi, H.; Miyashita, T.; Yamato, K.; Yoshio, M. *Denki Kagaku* **1993**, *61*, 720.
(22) Li, W.; Reimers, J. N.; Dahn, J. R. *Phys. Rev.* **1992**, *B46*, 3236.
(23) Dahn, J. R.; von Sacken, U.; Juskow, M. W.; Al-Janabi, J. *J. Electrochem. Soc.* **1991**, *138*, 2207.
(24) Arai, H.; Okada, S.; Ohtsuka, H.; Ichimura, M.; Yamaki, J. *Solid State Ionics* **1995**, *80*, 261.
(25) Kanno, R.; Kubo, H.; Kawamoto, Y.; Kamiyama, T.; Izumi, F.; Takeda, Y. Y.; Takano, M. *J. Solid State Chem.* **1993**, *102*, 542.
(26) Rougier, A.; Gravereau, P.; Delmas, C. *J. Electrochem. Soc.* **1996**, *143*, 1168.
(27) Berbenni, V.; Massarotti, V.; Capsoni, D.; Riccardi, R.; Marini, A.; Antolini, A. *Solid State Ionics* **1991**, *48*, 101.
(28) Reimers, J. N.; Dahn, J. R.; Greedan, J. E.; Stager, C. V.; Liu, G.; Davidson, I.; Von Sacken, U. *J. Solid State Chem.* **1993**, *102*, 542.
(29) Zhecheva, E.; Stoyanova, R.; Gorova, M.; Alcántara, R.; Morales, J.; Tirado, J. L. *Chem. Mater.* **1996**, *8*, 1429.
(30) Zhecheva, E.; Stoyanova, R.; Gorova, M.; Alcántara, R.; Morales, J.; Tirado, J. L. *Ionics*, in press.
(31) Hedwig, G. R.; Liddle, J. R.; Reeves R. D. *Aust. J. Chem.* **1980**, *33*, 1685.
(32) *Gmelins Handbuch der Anorganischen Chimie*, 8 Auflage, B. 57, Tl. B, Lfg. 3, Springer-Verlag: Berlin, 1974; s 891.
(33) Strouse, J. *J. Am. Chem. Soc.* **1977**, *99*, 572.

an oxygen atmosphere. The samples derived from $LiNiCit_{3/4}$, LiNiCit and $LiNiCit_2$ will be denoted as ex-$^3/_4$-citrate, ex-monocitrate and ex-biscitrate oxides, respectively. For the sake of comparison, $LiNiO_2$ was obtained by a solid-state reaction between NiO and Li_2CO_3. For the latter sample, nickel hydroxide−carbonate and Li_2CO_3 (Ni:Li = l:1) were homogenized for 1 h in a planetary mill. The intimate mixture was heated to 500 °C in air with a heating rate of 1 °C/min and then annealed at 800 °C in an oxygen atmosphere for 20 and 40 h.

2.2. Methods. The lithium content of the samples was determined by atomic absorption analysis. The total amount of nickel was determined complexometrically and by atomic absorption analysis. The amount of Ni^{3+} ions in the oxide samples was determined by iodometric titration. The organic complexes were analyzed according to the standard procedure for C/H (as CO_2 and H_2O) and for N_2 by the Dumas method.

The X-ray phase analysis was alternatively performed with a DRON diffractometer (Russia) and a Siemens D5000 apparatus, using Cu Kα radiation. Unit cell parameters are obtained from least-squares fitting of all peak positions.

Infrared spectra were recorded on a Specord-75 (ex-GDR) spectrometer in KBr pellets or in Nujol mulls in the 4000−400 cm^{-1} range.

DTA and TG experiments were performed with a Paulik-Paulik-Erdey (MOM, Hungary) apparatus in air and samples weighing 150 mg each were used. DSC measurements were carried out on a Perkin-Elmer apparatus in air with a heating rate of 10 °C/min, samples weighing 1.5 mg each being used.

The EPR spectra were registered as the first derivative of the absorption signal with an ERS-220/Q spectrometer (ex-GDR) within the temperature range of 90−400 K. The g factors were established with respect to a Mn^{2+}/ZnS standard. For the determination of the amount of carbon in the decomposition products, carbon obtained by incomplete combustion of citric acid at 400 °C was used as a standard.

SEM analysis on powder samples coated with gold were carried out in a JEOL-5300 instrument with 25 kV accelerating voltage. The specific surface area of the samples was determined by the BET method using low-temperature nitrogen adsorption.

Electrochemical experiments were carried out in two-electrode, $Li/LiClO_4$(PC:EC)/Li_xNiO_2 cells. Electrodes using oxide samples as active material were prepared as 7 mm diameter pellets by pressing at 200 MPa a mixture of 80% of sample (ca. 12 mg) and 8% of EPDM copolymer and 12% carbon black (Strem 4N) to improve the mechanical and electronic conduction properties. Lithium electrodes consisted of a clean 7 mm diameter lithium metal disk. The electrolyte solution (1 M $LiClO_4$ in a 1:1 mixture of bidistilled PC and EC) was supported by porous glass-paper disks. All cell manipulations were carried out inside the glovebox (M. Braun) under argon atmosphere (water content < 2 ppm). The electrochemical measurements were obtained by a multichannel system MacPile alternatively working under potentiostatic and galvanostatic conditions. Prior to the potentiostatic experiments the cells were allowed to relax until the condition dV/dt < 1 mV/h was fulfilled. Step potential electrochemical spectroscopy (SPES) was carried out by using 10 mV steps. Current relaxation was recorded during 1 h at each step.

3. Results and Discussion

3.1. Characterization of the Lithium−Nickel−Citrate Precursors. The lithium−nickel−citrates obtained by freeze-drying of the corresponding aqueous solutions a−c are green voluminous powders which are XRD amorphous and have the following chemical composition: $LiNiCit_{3/4}{\cdot}xH_2O$, $LiNiCit{\cdot}xH_2O$, and $LiNiCit_2{\cdot}xH_2O$, where $x \sim 5$. For simplicity, these compositions will be further denoted as $LiNiCit_{3/4}$, LiNiCit, and $LiNiCit_2$.

The IR spectra of the Li−Ni citrate compositions show in the 1630−1570 and in 1430−1380 cm^{-1} spectral ranges the two characteristic bands due to the asymmetric, ν_{as}, and symmetric, ν_s, vibrations of the carboxylate group (Figure 1). This clearly indicates that the carboxylate groups are deprotonated. The positions of the two characteristic bands, as well as the separation between them, are given in Table 1. In addition, the ν_{as} and ν_s modes are split. Owing to the sensitivity of the ν_{as} and ν_s vibrations toward the mode of carboxylate coordination, Table 1 gives two typical examples for monodentate and bridging carboxylate CO_2^- coordination: $Ni(CH_2OHCOO)_2$ and $Li(CH_3COO){\cdot}2H_2O$, respectively.[34,35] Moreover, the same table compares the values ν_{as} and ν_s for lithium−nickel−citrates with that for cobalt analogues (LiCoCit and $LiCoCit_2$, respectively), where monodentate and bridging coordination of carboxylate groups is established.[30] It seems that for the all lithium−nickel−citrate compositions the carboxylate groups act as monodentate agent. For $LiNiCit_2$ composition, this suggestion is not surprising if we consider the crystal structure data on 1:2 metal−citrate (−3) complexes, $(NH_4)_4(Cu/Zn)(C_6H_5O_7)_2$:[36,37] two citrate ions are situated in the first coordination sphere of the metal ion, each of them participating with two monodentate carboxylate groups and with the hydroxyl group. For $LiNiCit_{3/4}$ and LiNiCit compositions, the lack of bridging coordination of CO_2^- does not correspond with the crystal structure data on 1:1 metal(II)−citrate(−3) and 4:3 Ni(II)−citrate(−4) complexes ($[Mn/Fe(H_2O)_6][Mn/Fe(C_6H_5O_7)_2(H_2O)]_2{\cdot}10H_2O$[38,39] and $[N(CH_3)_4]_5[Ni_4(C_6H_4O_7)_3(OH)(H_2O)]{\cdot}18H_2O$,[39] respectively).

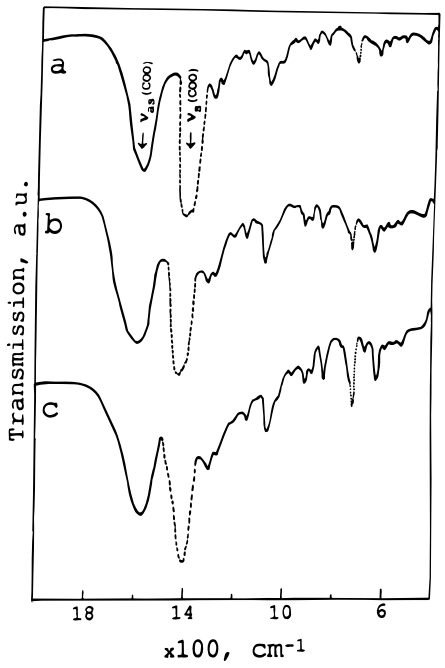

Figure 1. IR spectra of $LiNiCit_{3/4}$ (a), LiNiCit (b), and $LiNiCit_2$ (c). The spectra were recorded with Nujol mulls except for the spectral range 1500−1300 cm^{-1}, where KBr pellets are used.

(34) Nakamoto, K.; McCarthy P. J.; Miniatas, B. *Spectrochim. Acta* **1965**, *21*, 379.
(35) Cadene, M.; Vergnoux, A. M. *Spectrochim. Acta* **1972**, *A28*, 1663.
(36) Swanson, R.; Ilsey, W. H.; Stanislowski, A. G. *J. Inorg. Biochem.* **1983**, *18*, 187.
(37) Hott, R. C.; Sagatys, D. S.; Lynch D. E.; Smith, G.; Kennard, C. H. L.; Mak, T. C. W. *Aust. J. Chem.* **1991**, *44*, 1495.
(38) Glusker, J. P.; Carrell, H. L. *J. Mol. Struct.* **1973**, *15*, 151.
(39) Strouse, J., S. W. Layten, S. W.; Strouse, C. E. *J. Am. Chem. Soc.* **1977**, *99*, 562.

Table 1. Carboxylate Stretching Frequencies in Lithium−Citrate Compositions

samples	antisym str ν_{as}(COO), cm^{-1}		sym str, ν_s(COO), cm^{-1}		$\Delta\nu = \nu_{as} - \nu_s$, cm^{-1}	
$LiNiCit_{3/4}$	1627	1587	1413	1383	214	203
LiNiCit	1620	1587	1413	1383	207	204
$LiNiCit_2$	1615	1577	1400	1385	215	192
LiCoCit	1613	1570	1420	1394	193	176
$LiCoCit_2$	1607	1573	1420	1405	187	168
$Li(CH_3COO)\cdot 2H_2O$[a]	1597		1435		162	
$Ni(CH_2OHCOO)_2$[b]		1590		1403		187

[a]Reference 35. [b] Reference 34.

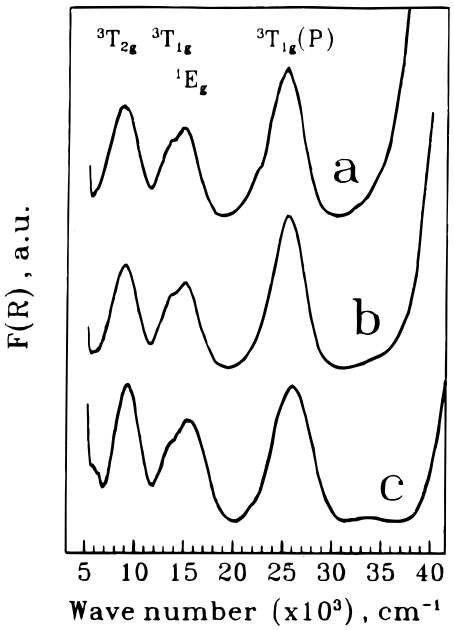

Figure 2. Diffuse reflectance spectra of $LiNiCit_{3/4}$ (a), LiNiCit (b), and $LiNiCit_2$ (c).

In the first case, the citrate ligand participates with two monodentate carboxylate groups and with one hydroxyl group, the pseudooctahedron being completed by 1 H_2O molecule and 2 β-carboxylate groups from neighboring citrate ligands.[38,39] In the second case, tetraionized citrate forms a large anionic complex with Ni(II) ions, in which two Ni_2 tetrahedral entities are joined together by bridging citrate carboxyl groups.[39]

Electronic spectra in the visible and near IR region were plotted to check the local surroundings of Ni^{2+} in the amorphous lithium−nickel−citrate precursors (Figure 2). For the three compositions, the diffuse reflectance spectra contain the absorption bands which are typical for octahedrally coordinated Ni^{2+}: $\nu_1(^3T_{2g}-{}^3A_2) \approx 9000\ cm^{-1}$; $\nu_2(^3T_{1g}-{}^3A_2 \approx 13\,700\ cm^{-1}$; $\nu_3(^3T_{2g}(P)-{}^3A_2) \approx 25\,500\ cm^{-1}$; the shoulder of the ν_2 band ($\approx 15\,000\ cm^{-1}$) is usually assigned as the $(^1E_g-{}^3A_2)$ transition (Figure 2). The positions of the absorption bands for the three compositions, as well as the positions of the electronic transitions for the Ni−aqua complex,[40] are summarized in Table 2. The complexation of Ni^{2+} with the citric acid is manifested by the shift of the absorption bands toward the higher energies as compared to that of $[Ni(H_2O)_6]^{2+}$ (Table 2). Using the crystal field formalism, Table 2 contains the values of the crystal field strength, *Dq*, and the Racah's parameter, *B*, for the Ni^{2+} ions in the compositions studied. The crystal field strength for Ni^{2+} increases in the following order: $H_2O < Cit_{3/4} < Cit < Cit_2$ (Table 2). The enhancement in crystal field strength for Ni^{2+} ions points to the appearance of Ni−citrate complexes with compositions depending on the Ni/Cit ratio. From this order it may be concluded that 4:3 Ni(II)−citrate(−4), 1:1 Ni(II)−citrate(−3) and 1:2 Ni(II)−citrate(−3) entities appear in $LiNiCit_{3/4}$, LiNiCit, and $LiNiCit_2$ compositions, respectively, where the coordination polyhedra of Ni^{2+} ions are completed by H_2O molecules and the Li^+ ions serve as counterions. However, for the 1:1 Co(II)−citrate(−3) complexes in the LiCoCit compositions, the citrate (−3) ligand leads to a weakness in the crystal field strength of Co^{2+} as compared to the H_2O ligand.[29,30] This opposite effect of the citrate (−3) ligand in the case of Ni(II)−citrate(−3) and Co(II)−citrate(−3) can be explained in terms of polynuclear−mononuclear equilibrium reactions which occur in concentrated solutions (0.5 M Ni/Co). As we have shown previously,[29] polynuclear Co(II)-citrate(−3) species predominate in the concentrated Co−citrate solutions. Obviously, in the Ni−citrate solutions, polymerization reactions do not take place and the 1:1 Ni(II)−citrate(−3) species are monomeric. This conclusion agrees well with the studies of Strouse,[33] who stated the presence of monomeric 1:1 Ni(II)−citrate(−3) complexes even in aqueous solutions with high ionic strengths. After freeze-drying of the 1:1:1 Li−Ni−citrate solution, the monomeric 1:1 Ni(II)−citrate(−3) complexes are preserved in the corresponding LiNiCit solid composition. The presence of monomeric 1:1 Ni(II)−citrate(−3) complexes gives an explanation of the IR data concerning the monodentate carboxylate coordination in LiNiCit composition.

Figure 3 shows the DTA and TG curves of the lithium−nickel−citrate compositions studied. For the three types of compositions, endothermic effects are observed between 100 and 170 °C, which are due to dehydration. As in the case of the thermal decomposition of other metal citrate salts,[41] the endo effects and the corresponding weight loss between 200 and 300 °C are to be explained by the transformation of the citrate to aconitate. Strong exothermic processes start at temperatures higher than 300 °C. For $LiNiCit_{3/4}$ and LiNiCit, the main weight loss appears in a relatively narrow temperature range, − 300−350 °C, whereas strong exothermic effects are observed up to 600 °C, the latter being accompanied with negligible weight changes. The high-temperature process (up to 600 °C) bears a resemblance to carbon combustion. The formation of residual carbon in the decomposition products of $LiNiCit_{3/4}$ and LiNiCit is related, most probably, to the low temperature, where the main decomposition process takes place. On the contrary, for $LiNiCit_2$ a continuous weight loss with the corresponding exo effects are

(40) Lever, A. B. P. *Inorg. Electron Spectrosc.* Elsevier: Dordrecht, 1984.

(41) Hennings, D.; Mayr W. *J. Solid State Chem.* **1978**, *26*, 329.

Table 2. d−d Transitions, Crystal Field Strength (*Dq*), and Racah's Parameter (*B*) for Octahedral Ni^{2+} in Lithium−Nickel−Citrate Compositions

	bands, cm^{-1}					
samples	$\nu_1(^3T_{2g}-^3A_2)$	$(^1E_g-^3A_2)$	$\nu_2(^3T_{1g}-^3A_2)$	$\nu_3(^3T_{2g}(P)-^3A_2)$	Dq, cm^{-1}	B, cm^{-1}
$LiNiCit_{3/4}$	8700	14 800	13 700	25 200	850	910
LiNiCit	8920	15 000	13 750	25 500	880	910
$LiNiCit_2$	9250	15 400	13 700	25 950	920	890
$Ni(H_2O)_6^{2+a}$	8500	15 200	13 800	25 300		930

[a]The data are taken from ref 40.

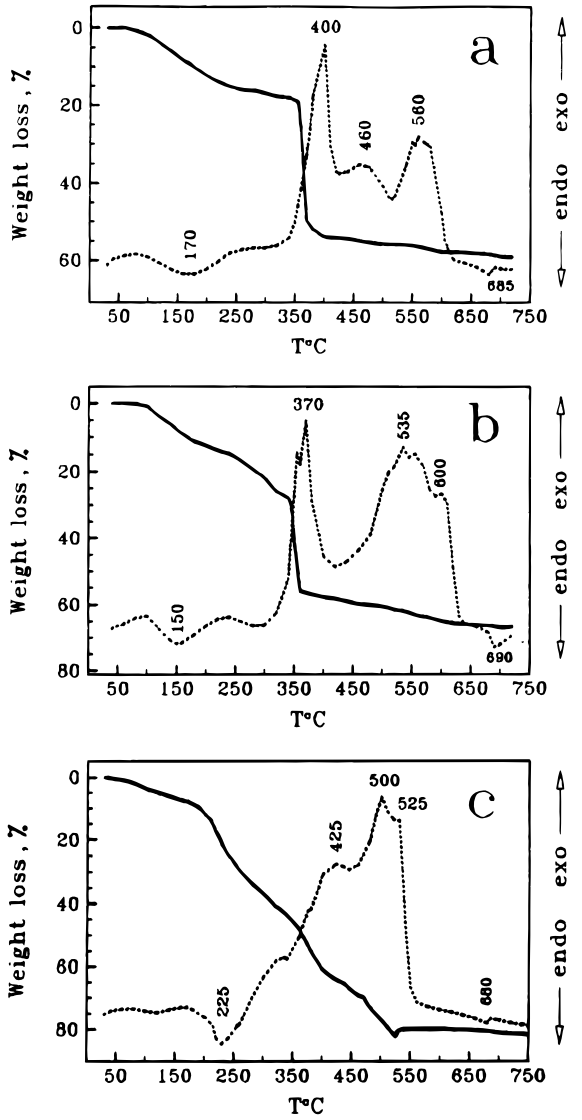

Figure 3. TG (full lines) and DTA (dotted lines) curves for $LiNiCit_{3/4}$ (a), LiNiCit (b), and $LiNiCit_2$ (c).

observed up to 550 °C. In addition, at 520 °C a slight increase in the weight of this sample is observed indicating the oxidation of metallic Ni. In addition, DTA curves for all compositions show a weak endothermic effect at 680−690 °C due to the melting of Li_2CO_3. At 600 °C, the phase composition of the products corresponds to a rock-salt phase (NiO) and Li_2CO_3.

Figure 4A shows the DSC curves during the decomposition of $LiNiCit_{3/4}$, LiNiCit, and $LiNiCit_2$. In accordance with the DTA results, the decomposition process for the three types of compositions starts at 350 °C but terminates at temperatures depending on the Ni/Cit ratio: the decomposition temperature increases as the Ni/Cit ratio decreases (Figure 4A). However, the total thermal effect of the combustion process is proportional on the number of carbon atoms: the thermal effect normalized per 1 C atom is 80 ± 5 cal/mol (Figure 4B).

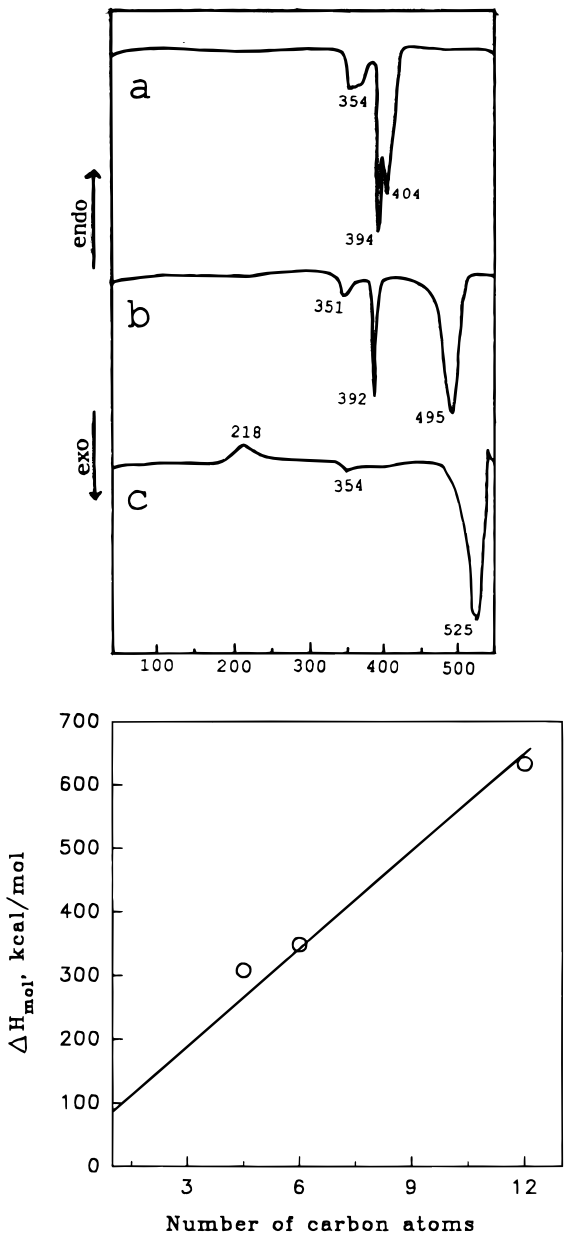

Figure 4. (A, top) DSC curves for $LiNiCit_{3/4}$ (a), LiNiCit (b), and $LiNiCit_2$ (c). (B, bottom) Heat of combustion, ΔH_{mol}, versus number of carbon atoms for the lithium−nickel citrate compositions.

3.2. Preparation and Structural Characterization of $LiNiO_2$. Irrespective of the conditions of decomposition (heating rate, atmosphere, and amount of decomposing sample), the thermal decomposition of Li−Ni−citrate salts at 450−650 °C always results in a mixture of lithium-containing NiO and Li_2CO_3. At-

tempting to obtain finely disperse layered $LiNiO_2$, we have established that the products of thermal decomposition of citrate salts at 500 °C in air are very appropriate precursors. These products represent a homogeneous mixture of lithium-containing NiO, Li_2CO_3, and residual carbon. The amount of lithium in NiO is insensitive toward the Ni/Cit ratio in the initial salt, but the carbon content decreases as the Ni/Cit ratio decreases in the initial salt. According to comparative EPR determination, the carbon amount is of 8, 3, and 0 wt % for ex-$^3/_4$-, ex-mono-, and ex-biscitrate oxides, respectively. The Ni/Cit ratio affects significantly the specific surface area of the decomposed products. The specific surface area decreases as the Ni/Cit ratio decreases: the specific surface area is of 18, 14, and 8 m^2/g for products obtained from $LiNiCit_{3/4}$, LiNiCit, and $LiNiCit_2$, respectively. The changes in the specific surface area are related to the different heat of combustion of $LiNiCit_{3/4}$, LiNiCit, and $LiNiCit_2$ compositions (Figure 4B).

Annealing the citrate precursors at 700−800 °C under oxygen leads to the formation of $Li_{1-x}Ni_{1+x}O_2$ oxides whose composition depend on the Ni/Cit ratio in the initial citrate salt (Table 3). At 700 °C, almost stoichiometric $Li_{1-x}Ni_{1+x}O_2$ oxides with $x \approx 0.05$ are obtained from mono citrate precursors, while the products of $^3/_4$- and biscitrate precursors are $Li_{1-x}Ni_{1+x}O_2$ with $x < 0.2$ after 40 h (Table 3). The deviation from the stoichiometry is lower for the oxides prepared at 800 °C and the most stoichiometric $Li_{1-x}Ni_{1+x}O_2$ is derived from monocitrate precursors, as in the case of oxides obtained at 700 °C (Table 3). The observed dependence of the stoichiometry of $Li_{1-x}Ni_{1+x}O_2$ on the Ni/Cit ratio results from the reactivity of the reaction mixture: high specific surface area and low carbon content favors the solid-state reaction between lithium-containing NiO and Li_2CO_3. Moreover, the reaction between lithium-containing NiO and Li_2CO_3 from citrate precursors yields at lower temperature and for shorter heating time more stoichiometric $Li_{1-x}Ni_{1+x}O_2$ as compared to $Li_{1-x}Ni_{1+x}O_2$ obtained by the ceramic method from NiO and Li_2CO_3 (Table 3).

As was mentioned in the Introduction, all $Li_{1-x}Ni_{1+x}O_2$ samples with $x < 0.33$ possess the trigonal crystal structure ($R\bar{3}m$ space group, Figure 5). The unit-cell parameters a and c, which correspond to the metal−metal intra- and interlayer distances, respectively, reflect the changes in the oxide stoichiometry (Figure 6a): a and c decrease as the lithium deficiency decreases. As a result, the c/a ratio, denoting the degree of trigonal distortion of the cubic cell, increases with the decreasing of x (Figure 6b). The changes observed in the unit-cell parameters match the different ionic radius of Li^+, Ni^{2+}, and Ni^{3+} and reveal the stabilization of two-dimensionality of the crystal lattice (Figure 6). These results agree with the literature data considering the effect of the nonstoichiometry on the lattice parameters of $Li_{1-x}Ni_{1+x}O_2$.[22] Furthermore, the unit-cell parameters for $Li_{1-x}Ni_{1+x}O_2$ with one and the same x values are sensitive toward the synthesis temperature: extrapolating x to 0, one obtains $a_{x\to0} = 2.8737 \pm 0.0007$ Å, $c_{x\to0} = 14.1889 \pm 0.0020$ Å and $a_{x\to0} = 2.8751 \pm 0.0005$ Å, $c_{x\to0} = 14.1896 \pm 0.0020$ Å for samples prepared at 700 and 800 °C, respectively. These parameters allow us to evaluate the degree of trigonal

Table 3. Chemical Composition (x in $Li_{1-x}Ni_{1+x}O_2$), Unit-Cell Parameters ($a \pm 0.0006$ Å and $c \pm 0.0018$ Å), Intensity Ratio between (003) and (104) Diffraction Peaks (I_{003}/I_{104}), Intensity Ratio between {(102) + (006)} and (101) Diffraction Peaks ($I_{102,006}/I_{101}$) for Lithium−Nickel Oxides Obtained at 700 and 800 °C with Heating Time of 20 and 40 h from Different Citrate Precursors[a]

	700 °C								800 °C							
temp	20 h				40 h				20 h				40 h			
time																
precursor	$LiNiCit_{3/4}$	LiNiCit	$LiNiCit_{0.05}$	$LiNiCit_2$	$LiNiCit_{3/4}$	LiNiCit	$LiNiCit_{0.05}$	$LiNiCit_2$	$LiNiCit_{3/4}$	LiNiCit	$LiNiCit_{0.05}$	$LiNiCit_2$	NiO Li_2CO_3	$LiNiCit_{3/4}$	LiNiCit	$LiNiCit_2$	NiO Li_2CO_3
x	0.221	0.098	0.118	0.257	0.088	0.054	0.090	0.124	0.038	0.033	0.049	0.086	0.131	0.076	0.048	0.083	0.056
a, Å	2.8871	2.8788	2.8785	2.8879	2.8792	2.8772	2.8767	2.8821	2.8779	2.8772	2.8766	2.8803	2.8838	2.8792	2.8790	2.8809	2.8789
c, Å	14.1978	14.1843	14.1869	14.2100	14.1909	14.1883	14.1802	14.1879	14.1896	14.1902	14.1933	14.1876	14.1921	14.1882	14.1901	14.1942	14.1887
c/a	4.918	4.927	4.928	4.920	4.929	4.931	4.929	4.923	4.931	4.932	4.934	4.926	4.921	4.928	4.929	4.927	4.928
I_{003}/I_{104}	0.69	1.06	0.93	0.66	1.14	1.21	1.08	0.93	1.23	1.59	1.29	1.00	1.00	1.16	1.30	1.07	1.05
$I_{006,102}/I_{101}$	0.813	0.511	0.519	0.898	0.519	0.495	0.510	0.649	0.481	0.447	0.447	0.738	0.645	0.467	0.591	0.538	0.454

[a] For comparative purposes, the samples obtained at 800 °C from mixtures of Li_2CO_3 and NiO are also included.

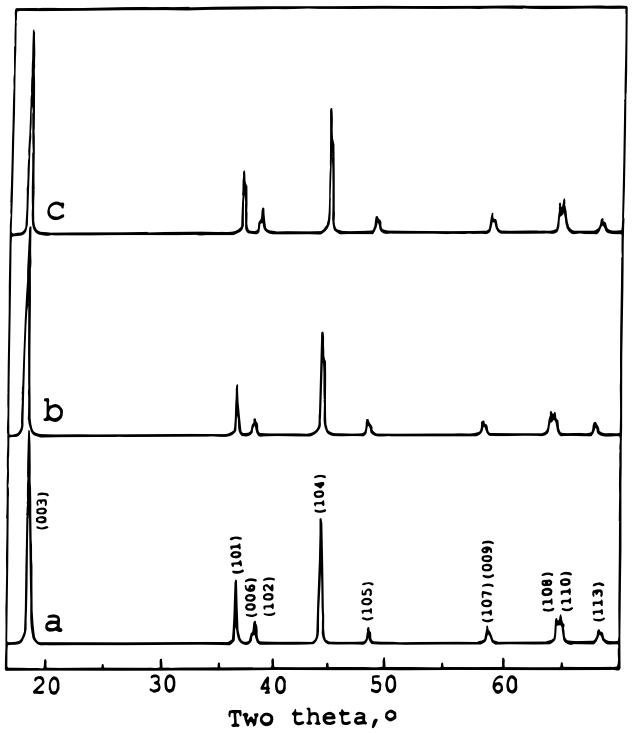

Figure 5. XRD patterns of ex-monocitrate $LiNiO_2$ obtained at 700 °C for 40 h (a) and at 800 °C for 20 h (b). For the sake of comparison, the XRD patterns of $Li_{1-x}Ni_{1+x}O_2$, obtained by a solid-state reaction between NiO and Li_2CO_3, at 800 °C for 40 h (c) is also given.

distortion of the cubic cell: $c/a_{x\to 0} = 4.937$ and $c/a_{x\to 0} = 4.935$ for $Li_{1-x}Ni_{1+x}O_2$ samples obtained at 700 and 800 °C, respectively. For the sake of comparison, at 700 °C, the value of the c/a ratio extrapolated for the stoichiometric $LiNiO_2$ coincides well with that determined experimentally for $Li_{0.995}Ni_{1.005}O_2$ obtained by use of a 4-fold excess of lithium: $c/a = 4.937$.[24] To the best of our knowledge, stoichiometric lithium−nickel compositions have not been obtained at 800 °C. The sensitivity of the unit-cell parameters on the preparation temperature can be related to disorder reactions in oxides obtained at 700 and 800 °C.

Two models are used to describe the cation distribution in $Li_{1-x}Ni_{1+x}O_2$. According to one of the models, the nickel in excess of the stoichiometric amount occupies the free sites in the LiO_2 layers, $[Li_{1-x}Ni_x][Ni]O_2$,[22] whereas according to the other model partial mixing of lithium and nickel in the "alien" layers (Li in NiO_2 and Ni in LiO_2 layers, respectively) occurs, $[Li_{1-x-\delta}Ni_\delta]$-$[Ni_{1-\delta}Li_\delta]O_2$.[22,42] In the case of almost stoichiometric $Li_{1-x}Ni_{1+x}O_2$ the first model is considered to be more reliable. Nevertheless, some cation mixing (δ is about of 5%) has been reported for oxides with $x = 0.04$.[22] Owing to the small scattering factor for Li, XRD method does not enable us to specify the reaction of intrinsic disorder in nearly stoichiometric $Li_{1-x}Ni_{1+x}O_2$.

In this respect no explicit information is given by IR spectroscopy on the cation distribution in $Li_{1-x}Ni_{1+x}O_2$. Regardless of the composition and the synthesis temperature, the IR spectra of all samples with a composition close to the stoichiometric consist of two intense bands at 500 and 560 cm^{-1} due to the vibrations of the NiO_2 layers (Figure 7).

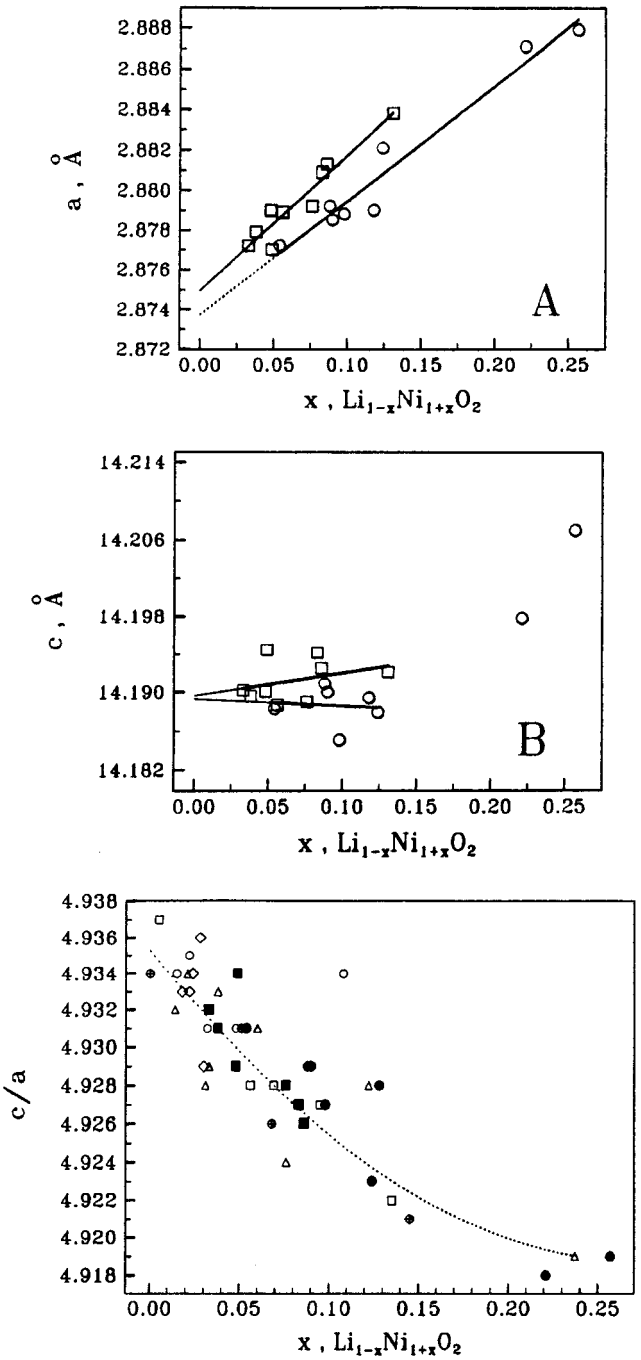

Figure 6. (a) Unit-cell parameters for the $R\bar{3}m$ space group, a (A) and c (B), for ex-citrate $Li_{1-x}Ni_{1+x}O_2$ obtained at 700 °C (○) and 800 °C (□). (b) c/a ratio versus chemical composition, x, for ex-citrate $Li_{1-x}Ni_{1+x}O_2$ obtained at 700 °C (●) and 800 °C (■). For the sake of comparison, data from ref 28 (○), ref 24 (Δ), ref 25 (◊), ref 26 (□) and ref 22 (⊕). The dotted line represents a fit for all literature data.

To differentiate the cation distribution in ex-citrate $Li_{1-x}Ni_{1+x}O_2$, EPR of low-spin Ni^{3+} were used to study the nickel surroundings. As was shown in previous investigations, at temperatures above the critical, the low-spin Ni^{3+} ions determine the appearance of a single line (with a Lorentzian shape and $g = 2.137$) in the EPR spectrum of $Li_{1-x}Ni_{1+x}O_2$ with $0.6 < x < 1.0$.[43−45] The phonon modulation of anisotropic and anti-symmetric

(42) Morales, J.; Pérez-Vicente, C.; Tirado, J. L. *Mater. Res. Bull.* **1990**, *25*, 623.

(43) Stoyanova, R.; Zhecheva, E.; Angelov, S. *Solid State Ionics* **1993**, *59*, 17.

(44) Stoyanova, R.; Zhecheva, E.; Friebel, C. *J. Phys. Chem. Solids* **1993**, *54*, 9.

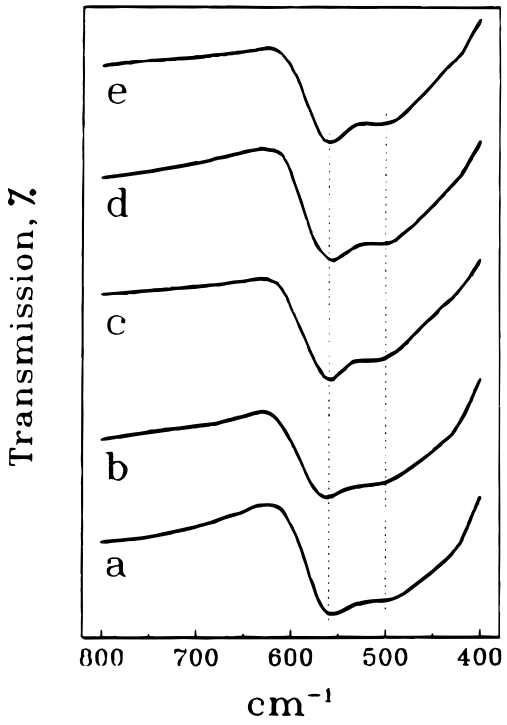

Figure 7. IR spectra of ex-monocitrate $Li_{1-x}Ni_{1+x}O_2$ obtained at 700 °C for 20 h (a), at 700 °C for 40 h (b), at 800 °C for 20 h (c), at 800 °C for 40 h (d). For the sake of comparison the IR spectrum of $Li_{1-x}Ni_{1+x}O_2$ obtained by a solid-state reaction between NiO and Li_2CO_3 at 800 °C for 40 h (e) is also given.

spin−spin interactions cause linear broadening of the Lorentzian line. The slope of linear dependence, $d\Delta H_{pp}/dT$, is proportional to the isotropic exchange integral, to the coordination number of the exchange-coupled particles and to the distance and angle between them. Thus, the different values of the $d\Delta H_{pp}/dT$ coefficients for partially ordered $Li_{0.6}Ni_{1.4}0_2$, and for layered $Li_{0.96}Ni_{1.04}O_2$ ($d\Delta H_{pp}/dT = 2.3$ and $d\Delta H_{pp}/dT = 0.39$ mT/K, respectively) correspond to the different strength of the $Ni^{3+}-O-Ni^{2+}$ magnetic interactions with 180° configuration and of the $Ni^{3+}-O-Ni^{3+}$ magnetic interactions with 90° configuration (critical temperature 210 and 6 K, respectively).[43−45] Figure 8 shows the temperature dependence of the line width, ΔH_{pp}, of the ex-citrate $Li_{1-x}Ni_{1+x}O_2$. The values of the $d\Delta H_{pp}/dT$ coefficients as functions of the oxide stoichiometry are summarized in Figure 9. As one can see, lithium deficiency, which is compensated by Ni^{2+}, gives rise to the $d\Delta H_{pp}/dT$ coefficient. At the samples with the same compositions, there is a clear dependence of the $d\Delta H_{pp}/dT$ coefficient on the synthesis temperature: $d\Delta H_{pp}/dT_{x\to 0} = 0.26$ and $d\Delta H_{pp}/dT_{x\to 0} = 0.42$ mT/K for the samples obtained at 700 and 800 °C, respectively. This result stress on the cation disorder in oxides obtained at 700 and 800 °C. The dependence of the $d\Delta H_{pp}/dT$ coefficient on the synthesis temperature may be explained by a model that accounts for the contribution of Ni^{2+} and Li^+ ions to the intralayer $Ni^{3+}-O-Ni^{3+}$ exchange interactions. With decreasing amount of Ni^{2+} ions (increasing amount of Li^+), the effect of the strong $Ni^{3+}-O-Ni^{2+}$ magnetic interactions is reduced, as a result of which the values of the $d\Delta H_{pp}/dT$ coefficient decrease smoothly. This relationship is observed with samples obtained at 700

(45) Stoyanova, R.; Zhecheva, E.; Friebel, C. *Solid State Ionics* **1994**, *73*, 1.

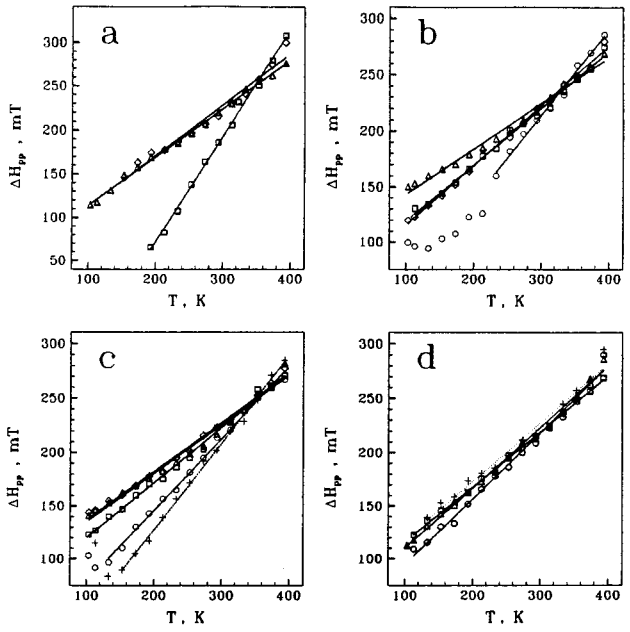

Figure 8. Temperature dependence of the EPR line width, ΔH_{pp}, for ex-citrate $LiNiO_2$ obtained at 700 °C for 20 h (a), at 700 °C for 40 h (b), at 800 °C for 20 h (c), at 800 °C for 40 h (d). (□) ex-$LiNiCit_{3/4}$, (△) ex-LiNiCit; (◊) ex-LiNiCit (0.05 M Ni); (○) ex-$LiNiCit_2$, (+) ex-carbonate $LiNiO_2$.

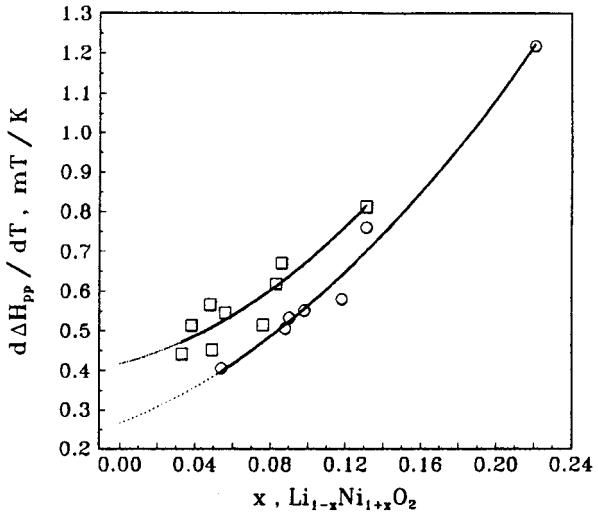

Figure 9. $d\Delta H_{pp}/dT$ coefficient versus chemical composition, x, for ex-citrate $Li_{1-x}Ni_{1+x}O_2$ obtained at 700 °C (○) and 800 °C (□).

°C (Figure 9). In this case, the extrapolating value of the $d\Delta H_{pp}/dT$ coefficient for stoichiometric $LiNiO_2$ ($d\Delta H_{pp}/dT_{x\to 0} = 0.26$ mT/K) would correspond to the "pure" 90° $Ni^{3+}-O-Ni^{3+}$ intralayer magnetic interactions. Disorder reactions produce two types of effects: (i) the presence of diamagnetic Li^+ ions in the magnetic NiO_2 layers disturbs the 90° $Ni^{3+}-O-Ni^{3+}$ intralayer interactions; (ii) the presence of Ni^{3+} ions in the LiO_2 layers induces l80° $Ni^{3+}-O-Ni^{3+}$ interlayer magnetic interactions, which is to be stronger as compared with the 90° $Ni^{3+}-O-Ni^{3+}$ intralayer magnetic interactions. This means that Li^+ and Ni^{3+} impurities in NiO_2 and LiO_2 layers, respectively, have opposite effects on the $d\Delta H_{pp}/dT$ coefficient: the Li^+ ions would reduce the $d\Delta H_{pp}/dT$ coefficient, while the Ni^{3+} ions would increase its values. Due to both effects, for stoichiometric $LiNiO_2$ with lithium disorder, the extrapolating value of the $d\Delta H_{pp}/dT$ coefficient does not match the $d\Delta H_{pp}/dT$ coefficient

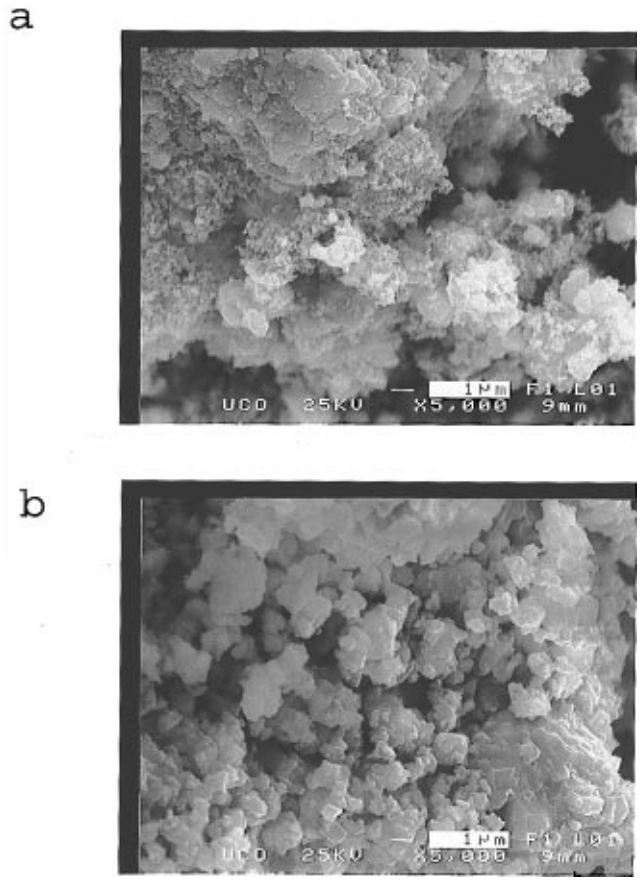

Figure 10. SEM micrographs of $LiNiO_2$ obtained from: LiNiCit at 700 °C for 40 h (a); LiNiCit at 800 °C for 20 h (b).

for stoichiometric $LiNiO_2$ with the ideal cation distribution. A similar dependence is observed with samples obtained at 800 °C where the extrapolating value of $d\Delta H_{pp}/dT$ coefficient ($d\Delta H_{pp}/dT_{x\to 0}$ = 0.46 mT/K) is higher than that determined for $LiNiO_2$ with "ideal" layered ordering (Figure 9). Hence, on the basis of the EPR study it may be concluded that, at 800 °C, the cation mixing is more significant than that for samples obtained at 700 °C. The lithium disorder observed in $Li_{1-x}Ni_{1+x}O_2$ obtained at 800 °C demonstrates that EPR of low-spin Ni^{3+} is a valuable tool for studying the reactions of intrinsic disorder in $Li_{1-x}Ni_{1+x}O_2$.

From scanning electron microscopy, it was observed that ex-citrate $Li_{1-x}Ni_{1+x}O_2$ powders possess a submicron particle size with a narrow particle size distribution. For samples prepared at 700 °C, the crystallite size is about 300 nm, whereas at 800 °C the particle size varies between 500 and 800 nm (Figure 10).

In conclusion it may be said that the lithium−nickel−citrate salts with Ni/Cit = 1 are very appropriate precursors for the preparation of nearly stoichiometric $Li_{1-x}Ni_{1+x}O_2$, $x \leq 0.05$, within the temperature range 700−800 °C. The cation distribution depends on the synthesis temperature: higher synthesis temperatures (800 °C) favor reactions of intrinsic disorder.

3.3. Electrochemical Performance of ex-citrate $LiNiO_2$ Electrodes. Figure 11 shows the SPES results of lithium anode cells using the ex-citrate $LiNiO_2$, sample obtained at 700 °C for 40 h as the active cathode material. The electrochemical behavior of $LiNiO_2$ electrodes has been examined in detail by different authors.[23−26,46−49] Thus, it is known that $LiNiO_2$ can be oxidized to $Li_{0.06}NiO_2$ without the destruction of its core

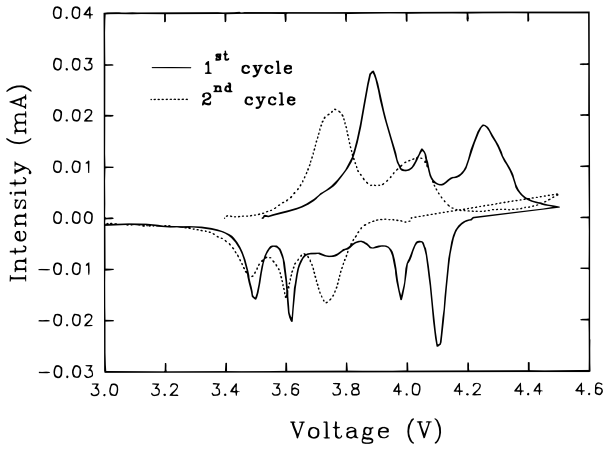

Figure 11. Step potential electrochemical spectroscopy voltammograms vs a pure lithium anode of ex-monocitrate $LiNiO_2$ samples obtained at 700 °C/40 h, recorded at 10 mV/h.

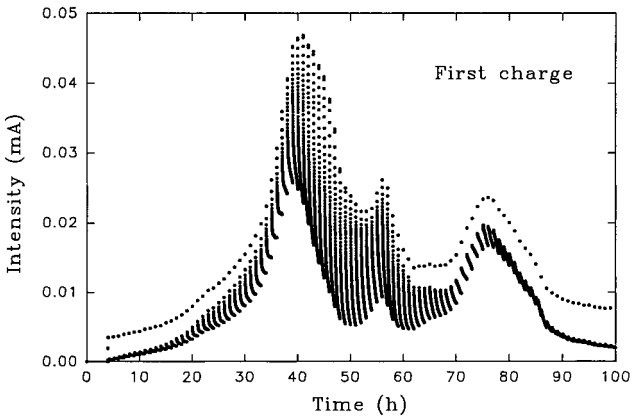

Figure 12. Current relaxation for potential steps in the 3.6−4.0 V interval during the charge of a lithium cell using the ex-citrate $LiNiO_2$ sample obtained from LiNiCit at 700 °C/40 h as cathode material.

structure.[46] Thus, the potentiostatic charge experiments were allowed to reach capacities close to that value. From Figure 11, a complex cell current vs voltage profile is observed with three main oxidation peaks located at 3.88, 4.05, and 4.25 V. After initial interpretations based on a single-phase process, it is now firmly established[46,47] that lithium extraction from $LiNiO_2$ takes place through three coexisting-phase regions. These regions are the result of three first-order transformations: hexagonal to monoclinic, monoclinic to hexagonal, and hexagonal to hexagonal.[47] The SPES peaks evidenced in Figure 11 show a direct correspondence with those reported in the literature by differential chronopotentiometry[46,47] and cyclic voltammetry[48] techniques. In addition, the SPES technique allows us to visualize the current relaxation in the voltage steps corresponding to lithium ion diffusion in single-phase electrodes as compared with phase transformation regions (Figure 12).

Besides, the nonstoichiometry of $Li_{1-x}Ni_{1+x}O_2$ was shown to have a direct effect on the charge profile and

(46) Ohzuku, T.; Ueda, A.; Nagayama, M. *J. Electrochem. Soc.* **1993**, *140*, 1862.
(47) Li, W.; Reimers, J. N.; Dahn, J. R. *Solid State Ionics* **1993**, *67*, 123.
(48) Broussely, M.; Perton, F.; Labat, J.; Staniewicz, R. J.; Romero, A. *J. Power Sources* **1993**, *43−44*, 209.
(49) Moshtev, R. V.; Zlatilova, P.; Manev, V.; Sato, A. *J. Power Sources* **1995**, *54*, 329.

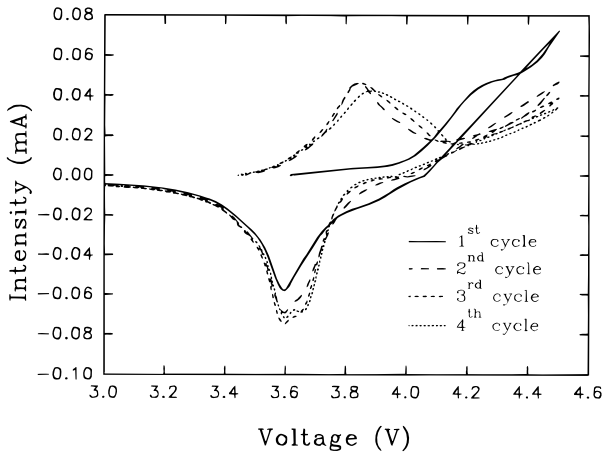

Figure 13. First four cycles obtained at 100 mV/h by step potential electrochemical spectroscopy of ex-monocitrate $LiNiO_2$ samples prepared at 700 °C/40 h, vs a pure lithium anode.

reversibility of the intercalation reaction.[24,26] While four steep peaks can be observed in incremental capacity plots of a nearly stoichiometric sample ($x = 0.005$), prepared by using an excess of lithium, larger x values did not allow their observation.[24] From the SPES results in Figure 11, it is worth noting that the cathodes prepared by thermal decomposition of the noncrystalline products of freeze-drying citrate solutions show a behavior that is clearly ascribable to a highly stoichiometric material, irrespective of the fact that no lithium excess was required during the preparation. This gives additional interest to the metal−organic precursor method in the lithium−nickel oxide system to obtain almost stoichiometric $LiNiO_2$ with high electrochemical performance.

On the other hand, it was recently shown that the shape of the charge−discharge profile changes significantly with the recording rate.[48] While the first cycle of the voltammetry of $LiNiO_2$ electrodes recorded at 30 mV/h which was reported by Broussley et al.[48] showed a profile that is highly coincident with the differential chronopotentiograms in previous works,[46,47] the different current peaks were not resolved in the cyclic voltammograms recorded at 300 mV/h. To confirm the effect of the voltammetry rate on the intensity profile, several experiments were carried out at different step sizes and relaxation times. A loss of peak resolution similar to that reported in previous works[48] was observed for 100 mV/h (Figure 13). Moreover, cell capacity showed a marked decrease on increasing scan rate. Thus, a discharge capacity of 210 mAh/g for the first cycle was found by using 10 mV/h, while ca. 60 mAh/g was the first cycle discharge value observed at 100 mV/h. However, the capacity retention was close to 100% even at the higher scan rate after the fourth cycle.

In addition, Broussely et al.[48] reported that the profile of the second cycle is not coincident with that observed during the first charge−discharge voltammogram for a scan rate of 300 mV/h. This result contrasts with the dx/dV plots reported by Li et al.,[47] in which several consecutive 100 h rate cycles were shown to give similar profiles. For ex-citrate samples, the shape of the second cycle recorded at 10 mV/h Figure 11 is not coincident with the first charge−discharge profile. The interpretation previously proposed[48] based on the structural transformation of the sample due to the lithium extraction from the lattice deserves further study. Thus, samples of cathode material were prepared after completion of the first cycle. After allowing 24 h relaxation of the cells, the cathode pellets were dismounted and XRD and EPR data were obtained. The comparison with the pristine cathode material reveals that the layered structure is preserved after cycling.

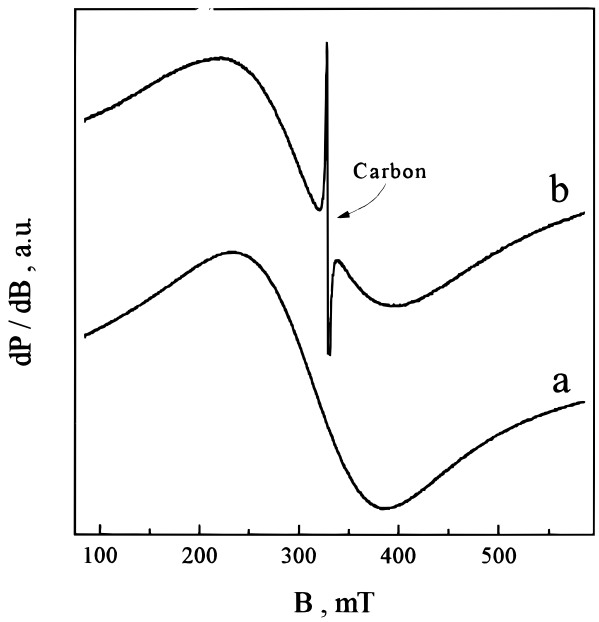

Figure 14. EPR spectra at 113 K of pristine (a) and cycled (b) $LiNiO_2$ compositions.

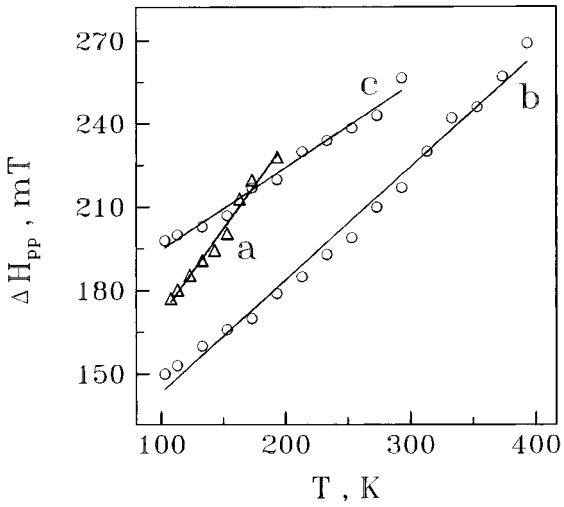

Figure 15. Temperature evolution of the EPR line width for $LiNiO_2$ after the first cycle (a). For comparison the temperature dependence of the EPR line width of Ni^{3+} for pristine composition (b) and chemically delithiated oxide, $Li_{0.79}Ni_{1.05}O_2$ (c), is also given.

EPR of low-spin Ni^{3+} gives further information on the cation distribution in $LiNiO_2$ after the first cycle. The EPR spectrum of cycled composition shows the same EPR signal as in the case of the pristine composition: a Lorentzian line with $g = 2.137$ due to the low-spin Ni^{3+} ions (Figure 14). The line width, ΔH_{pp}, decreases linearly as the registration temperature decreases, but the slope, $d\Delta H_{pp}/dT$, is higher in respect to the pristine composition: 0.64 and 0.40 mT/K for the cycled and pristine composition, respectively (Figure 15). For comparison, the same figure shows also the temperature dependence of the EPR line width for acid delithiated

$LiNiO_2$ having the composition close to that of cycled sample: $Li_{0.79}Ni_{1.05}O_2$.[50] As one can see, for the latter composition diamagnetic Ni^{4+} ions acting as charge compensators cause a line broadening and a reduction in $d\Delta H_{pp}/dT$ coefficient. For cycled composition, a line broadening is also observed, indicating the presence of Ni^{4+}. The occurrence of these ions is related to the unrecovered initial composition after the first cycle (Figure 11). However, the $d\Delta H_{pp}/dT$ coefficient for the cycled composition is significantly higher than that for acid-delithiated $LiNiO_2$. On the basis of the relationship between structure and EPR parameters of Ni^{3+} (described in the previous section), the increase in the $d\Delta H_{pp}/dT$ coefficient for the cycled composition is an indication for the appearance of Ni^{3+} in 3b sites (depleted lithium layers), which are involved into the strong antiferromagnetic 180° $Ni^{3+}-O-Ni^{3+}$ exchange interactions. The appearance of Ni^{3+} in lithium layers can be explained by the partial Ni migration from 3a (nickel layers) to 3b sites (lithium layers) during the lithium extraction/insertion reactions. Unfortunately, we are not able to estimate the amount of Ni^{3+} appearing in lithium layers, but it must be sufficiently high to perturb the ferromagnetic interactions in $LiNiO_2$: the Curie constants (estimated from the temperature dependence of the EPR signal intensity) are 90 and 50 K for the pristine and cycled composition, respectively. It must be emphasized that these EPR data are the first experimental evidence for nickel migration from 3a to 3b sites caused by complete lithium extraction.

(50) Alcántara, R.; Morales, J.; Tirado, J.-L.; Stoyanova, R.; Zhecheva, E. *J. Electrochem. Soc.* **1995**, *142*, 3997.

4. Conclusions

A metal−citrate method is elaborated for the preparation of finely dispersive layered $LiNiO_2$, which consists in thermal decomposition of homogeneous Li−Ni−citrate precursors. Freeze-drying of concentrated solutions with Li:Ni:citric acid = 1:1:0.75, 1:1:1, and 1:1:2 compositions leads to the formation of noncrystalline $LiNi(C_6H_4O_7)_{3/4}\cdot xH_2O$, $LiNi(C_6H_5O_7)\cdot xH_2O$, and $(NH_4)_3LiNi(C_6H_5O_7)_2\cdot xH_2O$ ($x \approx 5$) solids, respectively, were Ni^{2+} are complexed by citrate ions and Li^+ serve as counterions. The lithium−nickel−citrate salts with Ni/citrate = 1 are very appropriate precursors for the preparation of nearly stoichiometric submicron $Li_{1-x}Ni_{1+x}O_2$, $x \leq 0.05$, within the temperature range of 700−800 °C. The lower synthesis temperatures (700 °C) suppress the reactions of intrinsic disorder in the layers. The cathodes prepared from ex-monocitrate $LiNiO_2$ show a behavior that is clearly ascribable to a highly stoichiometric material, irrespective of the fact that no lithium excess was required during the synthesis. After the almost complete extraction of lithium, the capacity drop is related to a partial migration of Ni from 3a to 3b sites.

Acknowledgment. The authors express their gratitude toward the financial support of the European Union (Contract nr. ERB CIPD CT94 0501). R.A., P.L., and J.L.T. acknowledge financial support from CICYT (PB95-0561). R.A. is also indebted to UCO for a research grant.

CM970236A